NASA/TM-1998-208430

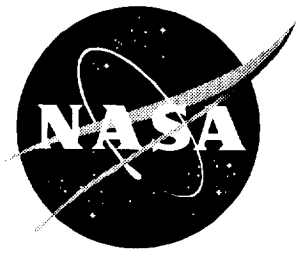

# An Evaluation of the Plasticity-Induced Crack-Closure Concept and Measurement Methods

*James C. Newman, Jr.*
*Langley Research Center, Hampton, Virginia*

National Aeronautics and
Space Administration

Langley Research Center
Hampton, Virginia 23681-2199

August 1998

Available from the following:

NASA Center for AeroSpace Information (CASI)
7121 Standard Drive
Hanover, MD 21076-1320
(301) 621-0390

National Technical Information Service (NTIS)
5285 Port Royal Road
Springfield, VA 22161-2171
(703) 487-4650

# AN EVALUATION OF THE PLASTICITY-INDUCED CRACK-CLOSURE CONCEPT AND MEASUREMENT METHODS

J. C. Newman, Jr.
NASA Langley Research Center
Hampton, Virginia
USA

## ABSTRACT

An assessment of the plasticity-induced crack-closure concept is made, in light of some of the questions that have been raised on the validity of the concept, and the assumptions that have been made concerning crack-tip damage below the crack-opening stress. The impact of using other crack-tip parameters, such as the cyclic crack-tip displacement, to model crack-growth rate behavior was studied. Crack-growth simulations, using a crack-closure model, showed a close relation between traditional $\Delta K_{eff}$ and the cyclic crack-tip displacement ($\Delta\delta_{eff}$) for an aluminum alloy and a steel. Evaluations of the cyclic hysteresis energy demonstrated that the cyclic plastic damage below the crack-opening stress was negligible in the Paris crack-growth regime. Some of the standard and newly proposed remote measurement methods to determine the "effective" crack-tip driving parameter were evaluated on middle-crack tension specimens. A potential source of the $K_{max}$ effect on crack-growth rates was studied on an aluminum alloy. Results showed that the ratio of $K_{max}$ to $K_c$ had a strong effect on crack-growth rates at high stress ratios and at low stress ratios for very high stress levels. The crack-closure concept and the traditional crack-growth rate equations were able to correlate and predict crack-growth rates under these extreme conditions.

## INTRODUCTION

In 1968, Elber observed that fatigue-crack surfaces contact each other even during tension-tension cyclic loading and he subsequently developed the crack-closure concept [1]. This observation and the explanation of crack-closure behavior revolutionized the damage-tolerance analyses and began to rationally explain many crack-growth characteristics, such as crack-growth retardation and acceleration. Since the discovery of plasticity-induced fatigue-crack closure, several other closure mechanisms have been identified, such as

roughness- [2] and oxide-induced [3] closure, which appear to be more relevant in the near-threshold regime. Recently, some researchers have questioned the validity of the crack-closure concept [4,5] and whether crack-tip damage occurs below the crack-opening stress [6,7]. Other measurement methods, from remote load-displacement records, are being proposed [6,7] to define an "effective" crack-tip damage parameter, other than the traditional effective stress-intensity factor range, $\Delta K_{eff}$. In addition, $K_{max}$-constant testing at extreme values (greater than 0.75 $K_c$) have produced very high crack-growth rates at extremely small values of $\Delta K$ [8]. Testing at high stress ratios, in the absence of crack closure, are producing different crack-growth rates at the same applied $\Delta K$ (or $\Delta K_{eff}$) value [9].

The objective of this paper is to make an assessment of the crack-closure concept, in light of some of these questions and assumptions. The paper will study the impact of using other crack-tip parameters, such as the cyclic crack-tip displacement $\Delta\delta_{eff}$ [10,11], or the cyclic crack-tip hysteresis energy $W^p_{eff}$ [12], to model crack-growth rate behavior and to assess the differences induced by using the $\Delta K_{eff}$ parameter. The $\Delta\delta_{eff}$ and $W^p_{eff}$ parameters are directly relatable to the effective cyclic J-integral [13]. Crack-growth simulations, using the modified Dugdale [14] crack-closure model [15,16], will be conducted over a wide range in stress ratios (R) to assess the impact of using cyclic crack-tip displacement as a crack-tip parameter. Some of the standard and newly proposed remote measurement methods to determine traditional crack-opening stresses or "effective" crack-driving parameters will be evaluated from the plasticity-induced crack-closure model analyses on middle-crack tension specimens. Analyses will be conducted under both constant-amplitude and single-spike-overload conditions. A potential source of the $K_{max}$ effects on crack-growth rate data will be studied at high stress ratios and at high stress levels on test data from an aluminum alloy.

## PLASTICITY-INDUCED CRACK CLOSURE MODEL

The plasticity-induced crack-closure model, shown in Figure 1, was developed for a through crack in a finite-width plate subjected to remote applied stress. The model was based on the Dugdale strip-yield model [14] but modified to leave plastically deformed

material in the wake of the crack. The details of the model are given elsewhere and will not be presented here (see Newman [15,16]). One of the most important features of the model is the ability to model three-dimensional constraint effects. A constraint factor, $\alpha$, is used to elevate the flow stress ($\sigma_o$) at the crack tip to account for the influence of stress state ($\alpha\sigma_o$) on plastic-zone sizes and crack-surface displacements. (The flow stress $\sigma_o$ is taken as the average between the yield stress $\sigma_{ys}$ and ultimate tensile strength $\sigma_u$ of the material.) For plane-stress conditions, $\alpha$ is equal to unity (original Dugdale model); and for simulated plane-strain conditions, $\alpha$ is equal to 3. Although the strip-yield model does not model the correct yield-zone shape for plane-strain conditions, the model with a high constraint factor is able to produce crack-surface displacements and crack-opening stresses quite similar to those calculated from three-dimensional, elastic-plastic, finite-element analyses of crack growth and closure for finite-thickness plates [17].

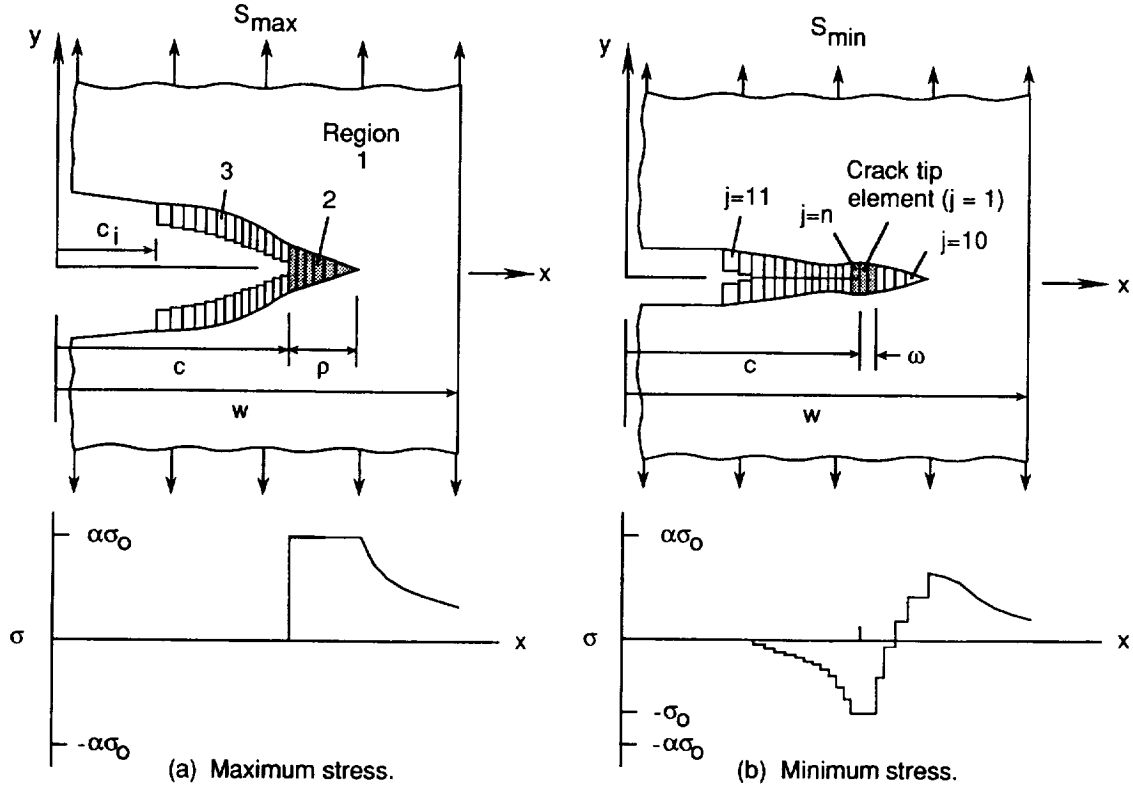


Figure 1. Schematic of strip-yield model at maximum and minimum applied loading.

The calculations performed herein were made with FASTRAN Version 3.0. The modifications made to FASTRAN-II (Version 2.0 described in reference 16) were made to improve the crack-opening stress calculations under variable-amplitude loading, to improve the element "lumping" procedure to maintain the residual plastic deformation history, and to improve computational efficiency. From the model, the crack-mouth opening displacements (CMOD) are calculated at the centerline of the model (x = 0). The cyclic crack-tip displacements and the cyclic hysteresis energy were calculated from the crack-tip element (j = 1) in Figure 1(b). The crack-opening stress, $S_o$, is calculated from the contact stresses shown in Figure 1(b), see references 15 or 16, by equating the applied stress-intensity factor at $S_o$ to the stress-intensity factor caused by the contact stresses. CMOD results under cyclic loading were used to determine the crack-opening stresses using the reduced-displacement or the compliance-offset methods, and an alternative effective stress-intensity factor range from the adjusted-compliance-ratio method [7].

## EFFECTIVE STRESS-INTENSITY FACTOR RANGE AGAINST CRACK-GROWTH RATE RELATIONS

The linear-elastic effective stress-intensity factor range developed by Elber [1] is

$$\Delta K_{eff} = (S_{max} - S_o)\, F \sqrt{(\pi c)} \qquad (1)$$

where $S_{max}$ is the maximum stress, $S_o$ is the crack-opening stress and F is the boundary-correction factor. The crack-growth rate equation proposed by Elber states that the crack-growth rate is a power function of the effective stress-intensity factor range (like the Paris equation), as shown by the dotted line in Figure 2. However, fatigue crack-growth rate data plotted against the $\Delta K$ or $\Delta K_{eff}$, commonly show a "sigmoidal" shape, as illustrated by the solid curve shown in Figure 2. To account for this shape, the power relation was modified by Newman [15] to

$$dc/dN = C\, (\Delta K_{eff})^n\ G / H \qquad (2)$$

where $G = 1 - (\Delta K_o/\Delta K_{eff})^p$ and $H = 1 - (K_{max}/C_5)^q$. The function G accounts for threshold variations with stress ratio ($\Delta K_o$ is a function of stress ratio) and the function H accounts for the rapid crack-growth rates approaching fracture. The parameter $C_5$ is the

cyclic fracture toughness. As cracked specimens are cycled to failure, the fracture toughness is generally higher than the toughness for cracks grown at a low load and then pulled to failure. This is caused by the shielding effect of the plastic wake [18]. The cyclic fracture toughness ($C_5$), like the elastic fracture toughness ($K_{Ie}$), is a function of crack length, specimen width, and specimen type. Nonlinear fracture mechanics methods, in general, are required to model the fracture process. Later, a two-parameter fracture criterion will be used to model the fracture process. A discussion of the threshold behavior is beyond the scope of the present paper. Thus, G is set to unity. Only the function H will be considered in the present analyses to account for non-closure induced $K_{max}$ effects.

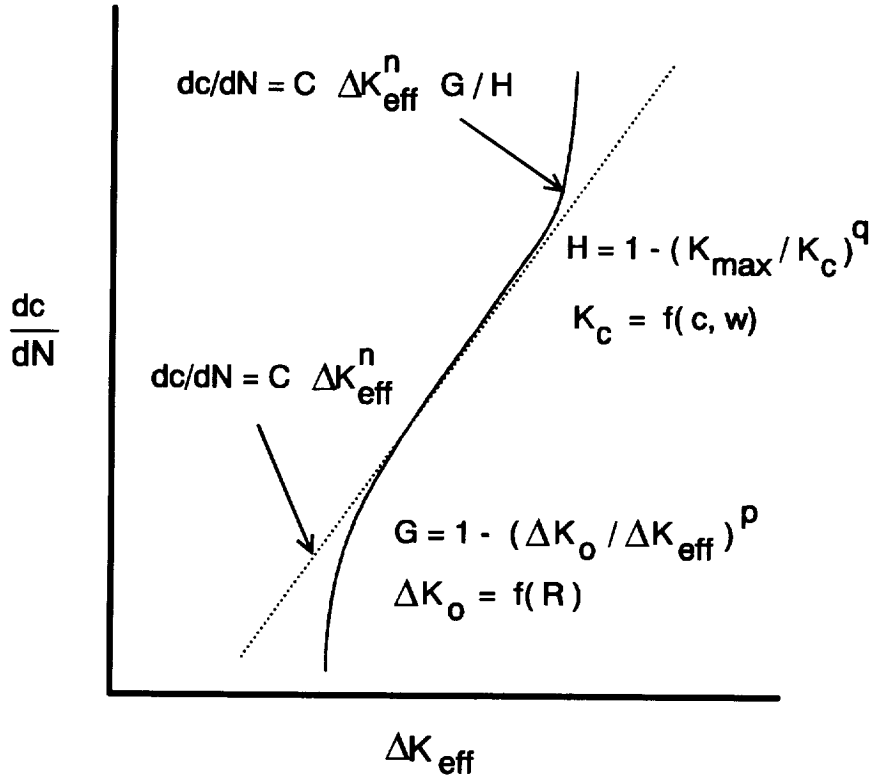


Figure 2. Schematic of effective stress-intensity factor against crack-growth rate relations showing influence of threshold and fracture toughness.

## CYCLIC HYSTERESIS ENERGY AND CYCLIC CTOD EVALUATIONS

In order to make an assess of the cyclic crack-tip damage for stresses below the traditional crack-opening stress, the cyclic plastic crack-tip displacements from the crack-tip element (j = 1) in Figure 1(b) was calculated for middle-crack tension M(T) specimens subjected to various

constant-amplitude loading conditions. The simulations were made on both 2024-T3 aluminum alloy and 4340 steel specimens. Some typical results on the aluminum alloy are shown in Figure 3. Here a constraint factor $\alpha = 2$ (near plane-strain conditions) was applicable at low crack-growth rates. This figure shows the applied stress plotted against the plastic crack-tip displacement for loading and unloading (no crack growth was allowed in the model during this load cycle). These results are quite similar to the remarkable experimental measurements made by Bichler and Pippan [19] on near crack-tip cyclic deformations. The solid symbol on the loading curve shows the crack-opening stress ($S_o$) and the arrow indicates the closure stress ($S_c$) during unloading. The traditional effective stress range, $\Delta S_{eff}$ was calculated from the difference between $S_{max}$ and $S_o$. The effective cyclic crack-tip displacement ($\Delta\delta_{eff}$) is given by the difference between the maximum and minimum plastic displacements. The total cyclic crack-tip hysteresis energy $W^p_{eff}$ was given by the area between the loading and unloading curves. The cross-hatched region is the cyclic

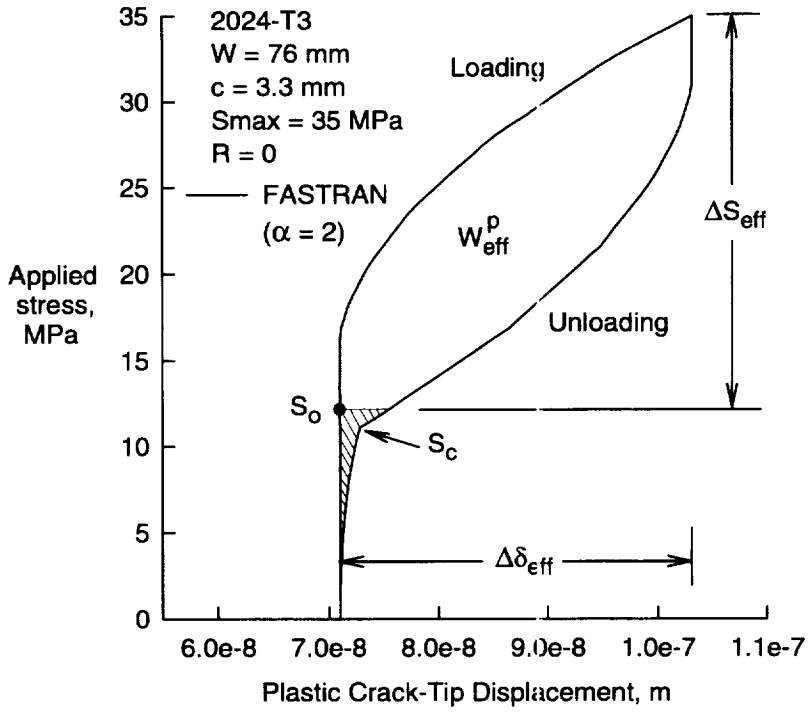


Figure 3. Calculated cyclic plastic crack-tip deformations under constant-amplitude loading.

plastic deformations that occur at applied stresses below the crack-opening stress. Thus, there is cyclic plasticity below the crack-opening stress. However, the cross-hatched area is a small percentage of the total (here it is only about 3.5 percent of the total area). For large-scale yielding conditions, the cross-hatched area becomes a larger percentage of the total, but here nonlinear fracture-mechanics parameters, such as $\Delta J_{eff}$, are needed to correlate crack-growth-rate data. However, for the Paris crack-growth regime, the effects of cyclic plasticity below the crack-opening stress on crack-growth rates is small and can be neglected. For the calculations made on the aluminum alloy and steel, the influence of cyclic plasticity below the opening load on crack-growth rates was estimated to be less than about 5 percent, assuming that crack-growth rates are nearly linearly related to the cyclic hysteresis energy.

The concept of using cyclic crack-tip displacements to characterize crack-growth rate behavior has been applied for many years (see Weertman [10] and Tomkins [11]). It is thought that the cyclic crack-tip displacement is a more fundamental parameter to characterize crack-tip damage. To evaluate the differences induced by using the traditional $\Delta K_{eff}$ concept, crack-growth simulations were made on aluminum alloy and steel specimens assuming that the material behaves under a simple power-law relation in terms of $\Delta K_{eff}$. The crack-growth constants for the two materials are given in Figure 4. The n-power on the aluminum alloy was 4 and the steel was 2. The respective constraint factors ($\alpha = 2$ for aluminum alloy and $\alpha = 2.5$ for steel) are the values needed to correlate stress-ratio data on these materials using $\Delta K_{eff}$. Simulations were made over a wide range in stress ratio (R = -1 to 0.8). Figure 4 shows the elastic modulus (E) times the effective cyclic crack-tip displacement ($\Delta\delta_{eff}$) plotted against the predicted crack-growth rate from $\Delta K_{eff}$. The results are remarkably linear over several orders of magnitude in rates with the slope on the aluminum alloy being 2 and the steel being unity. These results are reasonable because the crack-tip displacement is related to the square of the stress-intensity factor for small-scale yielding. But these results do show a slight spread in the results for various R ratios. The aluminum alloy would correlate within ±20 percent on rates whereas the steel would correlate within ±5 percent on rates. Part of this discrepancy may be due to neglecting the elastic contribution to the cyclic crack-tip displacement, in that, the high R ratio simulations would have had a slightly higher elastic displacement than the low R ratio results. (Rigid plastic

elements are used in the strip-yield model.) But, these results show that the traditional $\Delta K_{eff}$ and the effective cyclic crack-tip displacements are essentially equivalent concepts in the Paris crack-growth regime.

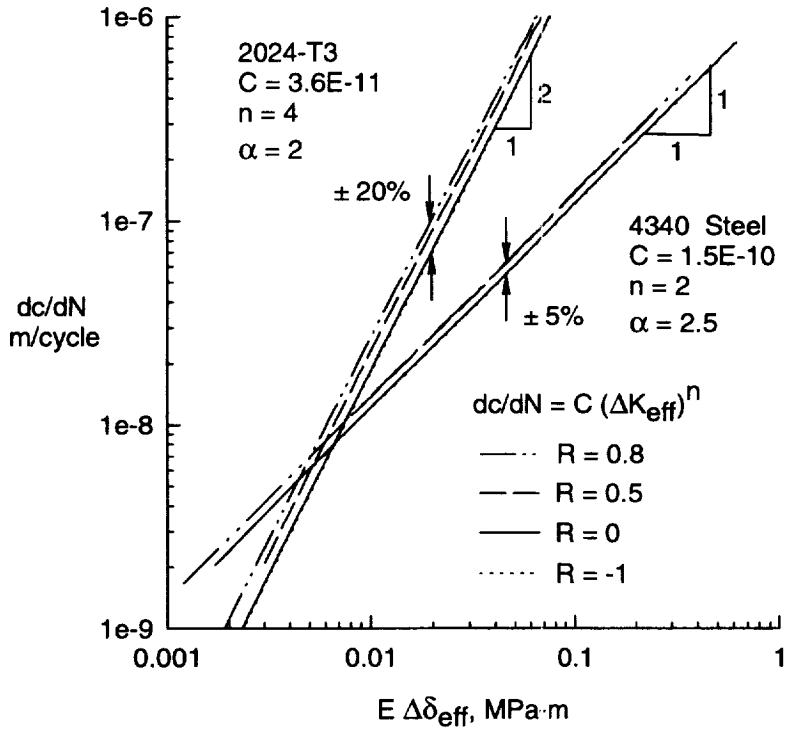


Figure 4. Calculated elastic modulus times effective cyclic crack-tip displacement against crack-growth rate for an aluminum alloy and steel for various stress ratios.

## REMOTE CMOD EVALUATIONS OF CRACK-TIP OPENING STRESSES AND EFFECTIVE STRESS-INTENSITY FACTOR RANGES

The ability to measure the true crack-opening load has been a very difficult task. Nonlinearities in displacement or strain measurement systems and electronic noise have contributed to this problem. In addition, the crack-closure process is three dimensional in nature with more closure occurring at and near the free surface than in the interior [20]. On the otherhand, the two-dimensional strip-yield or finite-element models have a unique crack-opening load. Thus, the 2D models may be used to study the various methods of determining the crack-opening loads and crack-tip parameters. But the 3D analyses are ultimately needed to assess the

best method to experimentally determine the most appropriate opening load to use in defining an effective crack-front parameter to characterize fatigue-crack growth (see Riddell et al. [21]).

In the following, the strip-yield model will be used to evaluate current and newly developed methods to determine either crack-opening loads or the effective stress-intensity factor ranges. Remote crack-mouth-opening displacements will be used to determine the crack-tip opening loads from reduced CMOD [22] and compliance-offset (ASTM E-647-95a) methods, and an alternative $\Delta K_{eff}$ from the adjusted-compliance-ratio method [7] under constant-amplitude loading. Comparison between measured and computed crack-opening loads will be made under a single-spike overload condition.

## Constant-Amplitude Loading

Reduced CMOD Method -- Crack-growth analyses were performed on a 2024-T3 aluminum alloy M(T) specimen under nearly plane-stress conditions ($\alpha = 1.2$) for constant-amplitude loading ($R = 0$). The CMOD traces from loading and unloading for three different crack lengths are shown in Figure 5. The solid symbols are the calculated crack-opening stresses $S_o$ determined from the contact stresses at minimum load. The $S_o$ values were essentially independent of crack length. These results illustrate why it is very difficult to determine the opening load from the very linear applied stress against CMOD records. Because there are global elastic deformations below the opening load for measurement method away from the crack tip, it is apparent why some researchers [6] have assumed that there is additional crack-tip deformations below the opening load.

As Elber [22] had pointed out many years ago, the reduced displacement technique is require to extract the crack-opening load from the nearly linear CMOD record. The applied stress against reduced CMOD are shown in Figure 6 for the largest crack length considered. The true opening load is obtained from the loading record when the loading curve becomes vertical. Again, the solid symbol is the opening load computed from the contact stresses at the minimum load. Here the computed opening load is slightly lower than the true opening load.

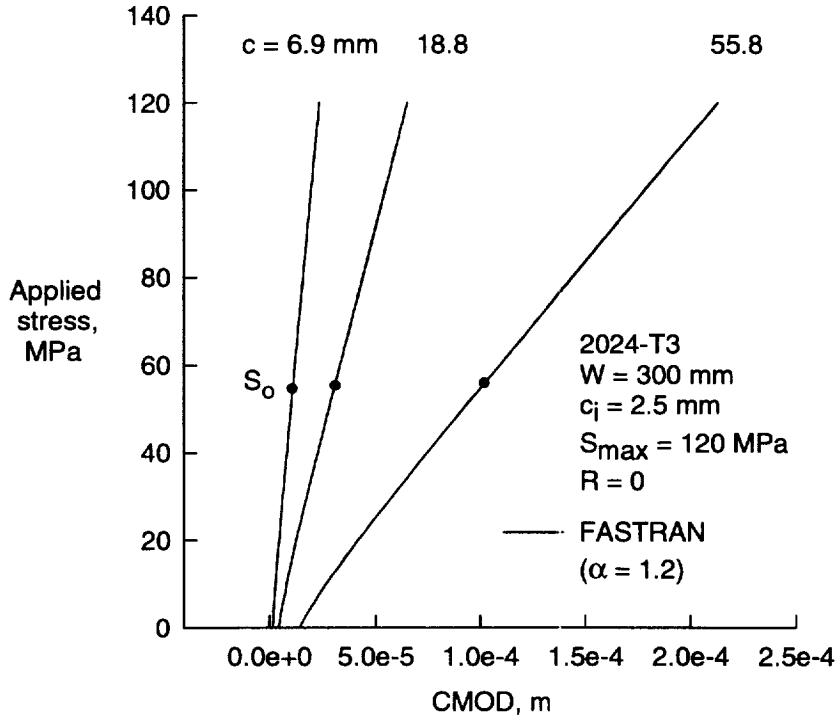


Figure 5. Calculated crack-mouth opening displacement under constant-amplitude loading for several crack lengths.

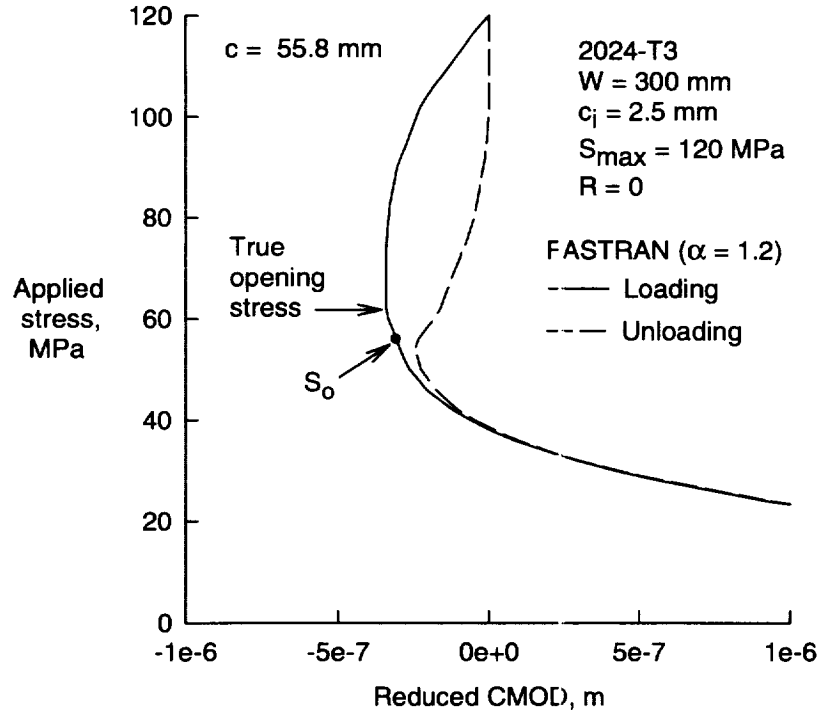


Figure 6. Calculated reduced crack-mouth opening displacement under constant-amplitude loading.

The crack-opening load determined from the reduced CMOD method from the 2D crack-growth simulations is independent of measurement location. Crack-opening loads determined from various local and remote measurement locations produced the same crack-opening loads. Thus numerically, the crack-opening load can be determined from any measurement location in a cracked body. However, from a testing standpoint, the amplification of the reduced CMOD record may be such that experimental noise may prevent reliable determination of the true opening load.

CMOD Compliance Offset Method -- Figure 7 shows the CMOD compliance offset record for the largest crack length considered in the previous example. The 1 and 2 percent offset values, commonly used in practice, produce crack-opening values that are considerably lower than the true opening stress. It is apparent from these calculations why the offset method is not able to correlate fatigue-crack-growth-rate data [7]. In addition, crack-opening loads from the 1 or 2 percent offset method have also been shown to be dependent upon the measurement location [7].

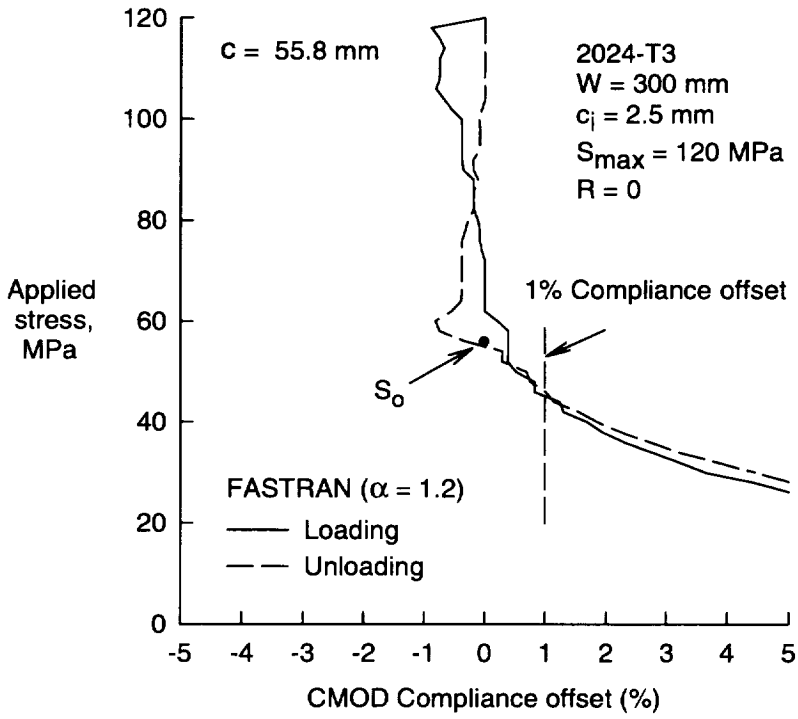


Figure 7. Calculated CMOD compliance offset under constant-amplitude loading.

Adjusted Compliance Ratio Method -- Recently, a new method to determine an effective stress-intensity factor range has been introduced to help overcome some of the difficulties with the compliance offset method. This method is called the Adjusted Compliance Ratio (ACR) method [23]. The ACR = $U_{ACR} = (C_s - C_i)/(C_o - C_i)$ where $C_s$ is the secant compliance (from minimum to maximum load), $C_o$ is the compliance above the opening load, and $C_i$ is the compliance prior to initiation of a crack. $C_i$ is assumed to be the compliance of the initial sawcut or notch in the specimen. The effective stress-intensity factor range is defined as $\Delta K_{eff} = U_{ACR}$ $\Delta K$. To compare $\Delta K_{eff}$ from ACR and the traditional crack-opening concept, a crack-growth simulation was performed on a M(T) specimen made of 2024-T3 aluminum alloy under nearly plane-stress conditions at $S_{max}$ = 120 MPa at R = 0. The specimen had an initial crack length (or sawcut) of 6.4 mm and a total width (W) of 76 mm. Figure 8 shows the U values plotted against crack length from ACR ($U_{ACR}$, dashed curve) and from crack-opening theory (solid curve) where $U_{op} = (K_{max} - K_o)/(K_{max} - K_{min})$. At crack length A, the U values are nearly equal and the rate is 1.1E-6 m/cycle based on equation (2). This is the reference point, since the U values and rates are equal. At crack length B, based on crack-opening theory, the rate reaches a minimum of 4.5E-7 m/cycle, and at crack length C the rate is 8E-7 m/cycle (rate is still less than that at point A). These changes in rate are consistent with experimental measurements made on 2024 aluminum alloy for a crack initiating at a sawcut or notch, see Broek [24]. However, the ACR method predicts that the rates at point B and C are greater than that at point A, since $\Delta K_{ACR}$ and $K_{max}$ values are greater at point B and C than at point A. Thus, the ACR method currently cannot explain the crack-growth transients for a crack initiating at a sawcut or notch. Whether the ACR method gives a more fundamental effective stress-intensity factor range than the traditional crack-closure concept must await further evaluations.

## Single-Spike Overload

Wu and Schijve [25] have measured crack-opening stresses under single-spike overloads and underloads using the reduced CMOD method. The crack-closure model was used to simulate crack growth under these conditions [26]. The predicted crack-growth

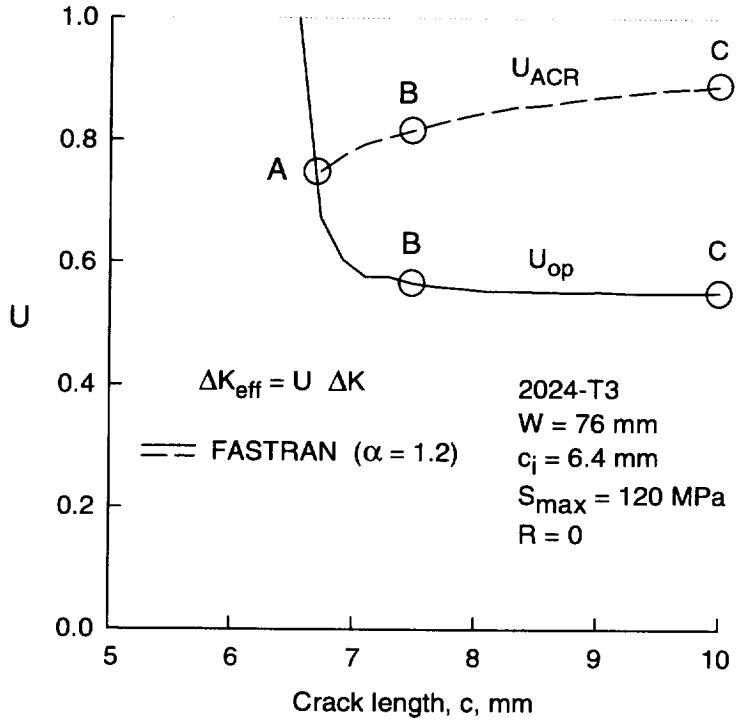


Figure 8. Calculated effective stress-intensity factors under constant-amplitude loading using traditional and adjusted compliance ratio methods.

delays due to overloads and underloads were in good agreement with the experimental measurements. Figure 9 shows the remote CMOD record for the spike overload simulation at some point after the application of the overload. The test was conducted at a constant-amplitude loading with $S_{max}$ = 100 MPa at R = 0 and a factor of two overload was applied when the crack reached 6 mm. The solid curve shows the calculated loading and unloading curves. The dashed line is the slope of the loading curve above the calculated crack-opening load (solid symbol). The range of measured crack-opening stresses are as indicated by the arrows. This range was lower than the calculated value but significantly above the value measured under constant-amplitude loading (about 40 MPa).

A comparison of calculated reduced CMOD for the constant-amplitude (dashed curve) and single-spike overload (solid curve) is shown in Figure 10. The solid symbol and arrow shows the crack-opening stress for constant-amplitude and spike overload, respectively. These results demonstrate why it may be easier to measure the opening loads under spike

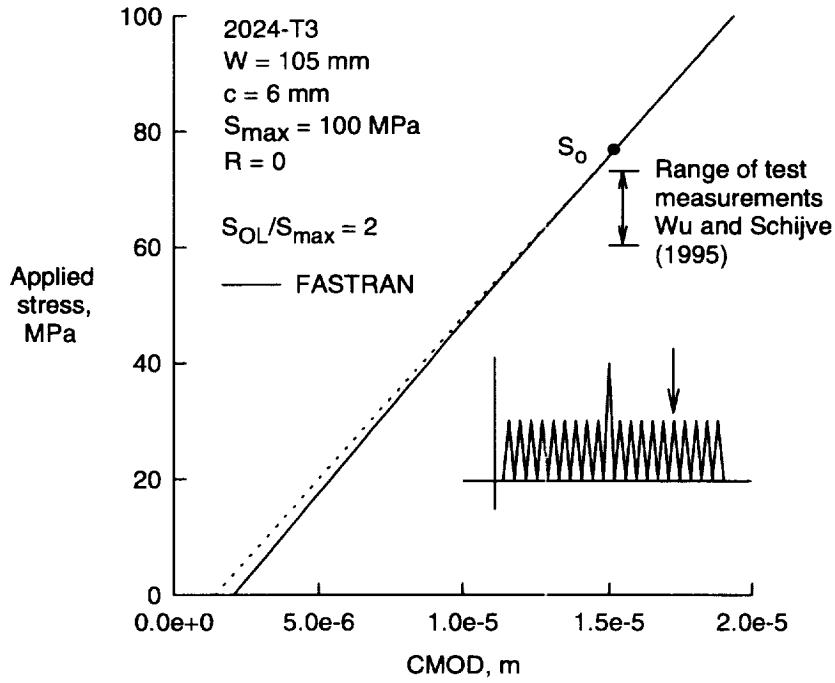


Figure 9. Calculated CMOD after a single-spike overload and comparison of measured and calculated crack-opening stresses.

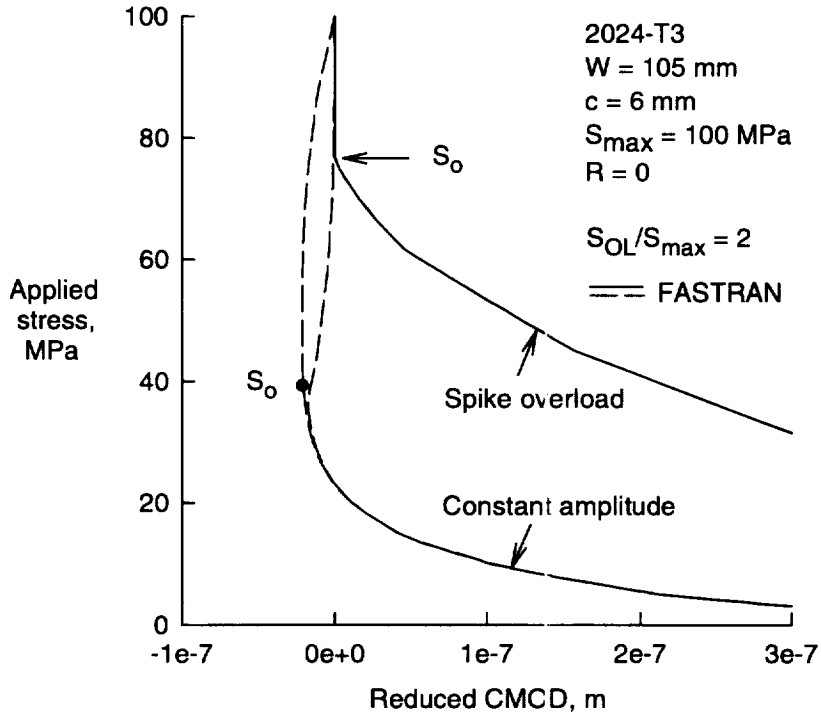


Figure 10. Comparison of reduced CMOD for constant-amplitude and single-spike overload conditions.

overloads because a large compliance change occurs when the crack surface separate following the spike overload.

## EFFECTS OF $K_{max}$ ON CRACK GROWTH IN ALUMINUM ALLOYS

In the last few years, the study of $K_{max}$ effects on crack-growth rates has intensified [4,7-9]. However, the study of these effects are not new, see Paris and Erdogan [27]. From the early 1960's, many researchers had seen these effects and they referred to them as $K_{max}$ or stress-level effects. Numerous equations have been proposed to account for these effects on crack-growth rates, even in the presence of crack closure. But why are researchers seeing more $K_{max}$ effects? First, specimen sizes that are being used in the laboratory are becoming smaller, tests are being conducted at very high R ratios (greater than 0.7), and $K_{max}$ values are approaching the elastic fracture toughness of the cracked specimen and material.

Herein, the $K_{max}$ effect will be studied on two sets of data on 2024 aluminum alloy. The first dataset is a recent study [9] on small, extended compact, EC(T), specimens (w = 76 mm) tested at low $\Delta K$ values but over a very wide range in stress ratios. The second dataset [28] was conducted on large M(T) specimens (W = 305 mm) at low and high R ratios but at extremely high stress levels (0.6 to 0.75 $\sigma_{ys}$).

The effective stress-intensity factor range against crack-growth rate data for the 2024-T3 aluminum alloy used in these two studies [9,28] is shown in Figure 11. These data were obtained from Hudson [29] and Phillips [30] over a wide range in stress ratio (symbols). An assessment of these data indicated that there were no $K_{max}$ effects in these data because of the low R ratios tested and that $K_{max}$ was less than 0.3 of the elastic fracture toughness for these tests. The solid curve is the baseline curve used in the subsequent analyses and the dashed curves show the scatter (±40 percent) that is typical of these type of data correlation. The data has been shown only over three orders of magnitude in rates because this covers the rate range measured by Riddell and Piascik [9] in their constant-$\Delta K$ tests. In the crack-growth analyses, equation (2) was used to model crack growth. Because transitions or slope changes occur in the data (such as the rate data below 1E-8 m/cycle), the coefficient C and power n are a function of rate range. Because large-crack thresholds are not relevant to the subsequent

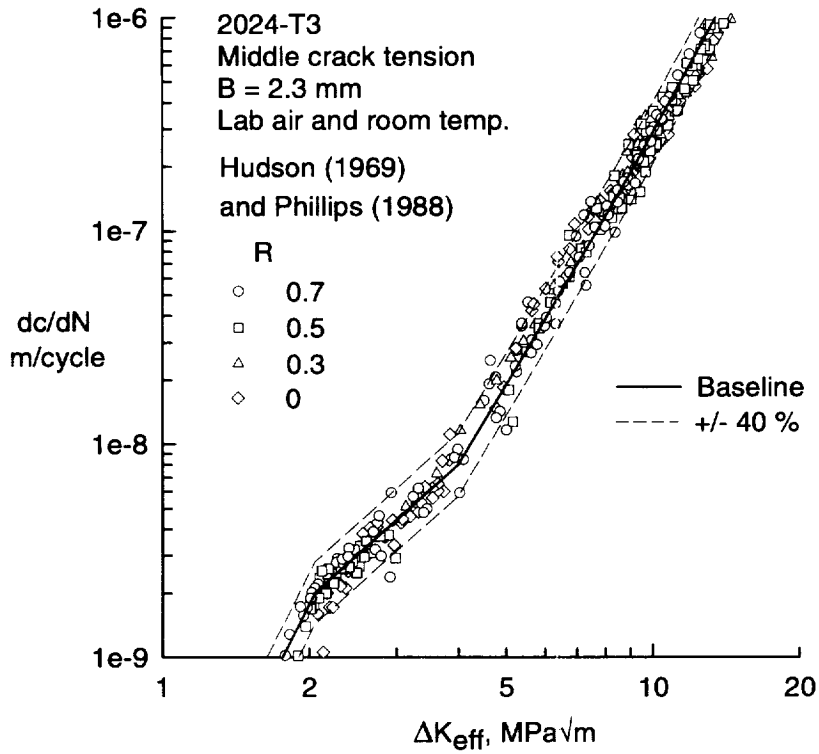


Figure 11. Effective stress-intensity factor range against crack-growth rate for a thin-sheet aluminum alloy for a wide range in stress ratios.

calculations and the subject is beyond the scope of the present paper, G = 1 in equation (2). The function, $H = 1 - (K_{max}/C_5)^q$, accounts for the rapid crack-growth rates observed as $K_{max}$ approaches the elastic fracture toughness. The parameter $C_5$ is the cyclic elastic fracture toughness, like $K_c$. But before the crack-growth analyses are made, methodology to predict the elastic fracture toughness, as a function of crack length and width, need to be considered.

The elastic fracture toughness ($K_{Ie}$) for compact C(T) specimens made of the 2024-T3 material is shown in Figure 12. $K_{Ie}$ is calculated from the initial crack length (before stable tearing) and the maximum failure load. (This is consistent with the way $K_{max}$ is calculated in current fatigue-crack-growth analyses.) The solid symbols are test data on C(T) specimens for various specimen widths (w). The solid curve is the Two-Parameter

Fracture Criterion (TPFC) [31] with a value of $K_F$ and m chosen to fit these data. The TPFC equation is

$$K_F = K_{Ie} / [1 - m (S_n/S_u)] \qquad \text{for } S_n < \sigma_{ys} \tag{3}$$

where $K_F$ and m are the two fracture parameters, $S_n$ is the nominal stress, and $S_u$ is the nominal stress at the plastic-hinge condition using the ultimate tensile strength ($\sigma_u$). The upper dotted curve is the values of $K_{Ie}$ at the plastic-hinge condition using the yield stress (nominal stress $S_n$ calculated at the crack tip is 1.61 $\sigma_{ys}$ under these conditions). The dashed curve is the condition when the nominal stress is equal to the yield stress. The open symbol shows the estimated elastic fracture toughness for a small extended compact specimen (w = 38.1 mm at $c_i/w = 0.4$). This value, $K_{Ie} = K_c = C_5 = 50$ MPa$\sqrt{m}$, will be used in the crack-growth analyses. For a given specimen width (w = 38.1 mm), the elastic fracture toughness is a function of crack length, as shown in Figure 13, for the extended compact specimen. The K solution for the extended compact specimen was obtained from

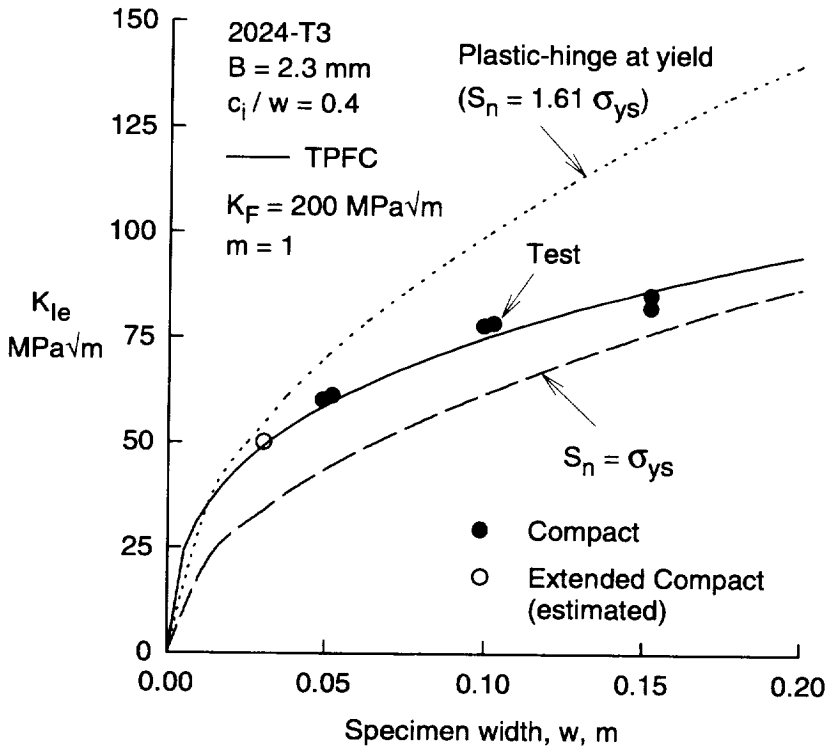


Figure 12. Elastic fracture toughness as a function of specimen width for compact specimens.

Piascik and Newman [32]. Here the value of $K_F$ and m from the compact specimens were used in the TPFC analysis to predict crack length effects for the extended compact specimen. The arrow along the c/w axis shows the range of testing in reference 9, and the solid symbol is the estimated elastic fracture toughness used in the crack-growth analyses. These results show that $K_{max}$ effects may intensify for larger crack lengths because the elastic fracture toughness drops sharply.

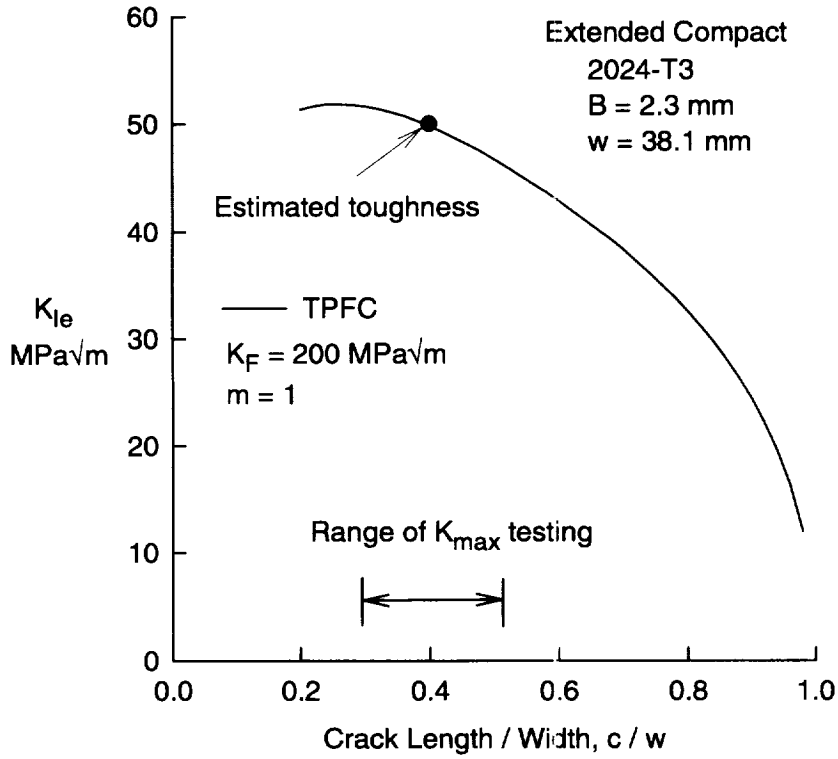


Figure 13. Calculated elastic fracture toughness for extended compact tension specimens.

Riddell and Piascik [9] tested small extended compact specimens under constant-ΔK values for a very wide range in stress ratios. Some typical results at 5.5 MPa√m are shown in Figure 14 as the solid symbols. The upper axis shows the ratio of $K_{max}/K_c$ for these test data. The solid curve is the predict results from equation (2) where the power on the $K_{max}/C_5$ ratio was q = 2. The power of q = 2 had been previously selected for aluminum alloys [15]. The dotted lines show the ±40 percent scatterband about the solid curve. All

of the test data fall within the scatterband. For comparison, the dashed curve shows the calculated results using only $\Delta K_{eff}$ without the $K_{max}$ term.

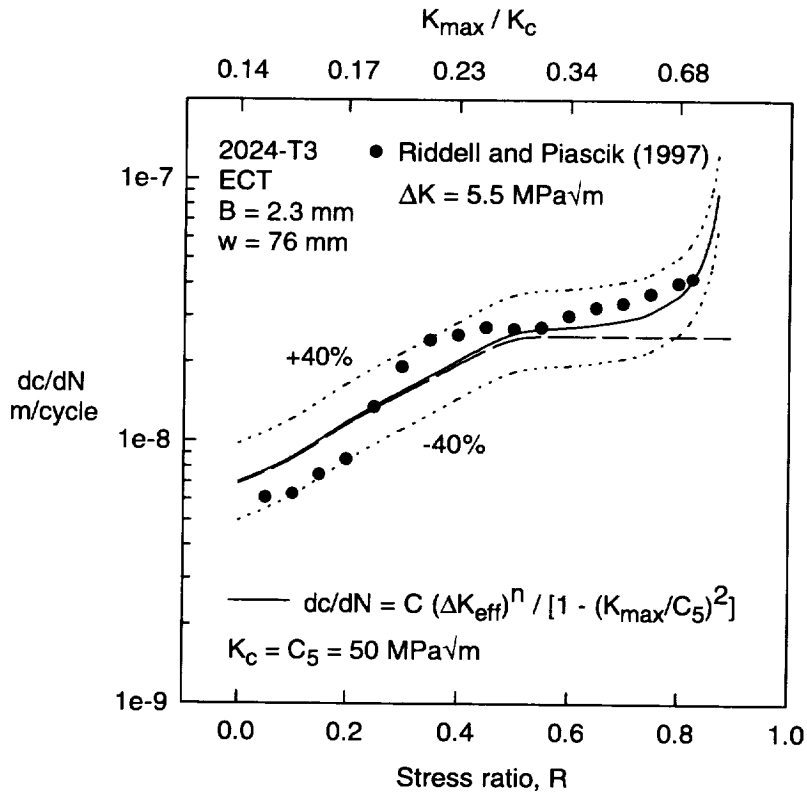


Figure 14. Comparison of measured and calculated crack-growth rates at constant ΔK value.

Figure 15 shows how different values of the power q affect the predicted crack-growth rates. When $q = \infty$, the $K_{max}$ term is eliminated, but when $q = 1$, rates are affected at all stress ratios. Because of the scatter in the test data, a q value of 1.5 to 2 seems to fit the data reasonably well. Constant-ΔK test results at lower and higher ΔK values are shown in Figure 16 with the predicted results from equation (2) with and without the $K_{max}$ term. Comparisons between test data and predict results (solid curves) are reasonable.

Dubensky [28] tested M(T) specimens (W = 305 mm) over a wide range in stress ratios (R = 0 to 0.7) and at extremely high values of applied stress (0.6 $\sigma_{ys}$ to $\sigma_{ys}$). For clarity, only some of his data (symbols) are shown in Figure 17 as ΔK plotted against measured rate. The

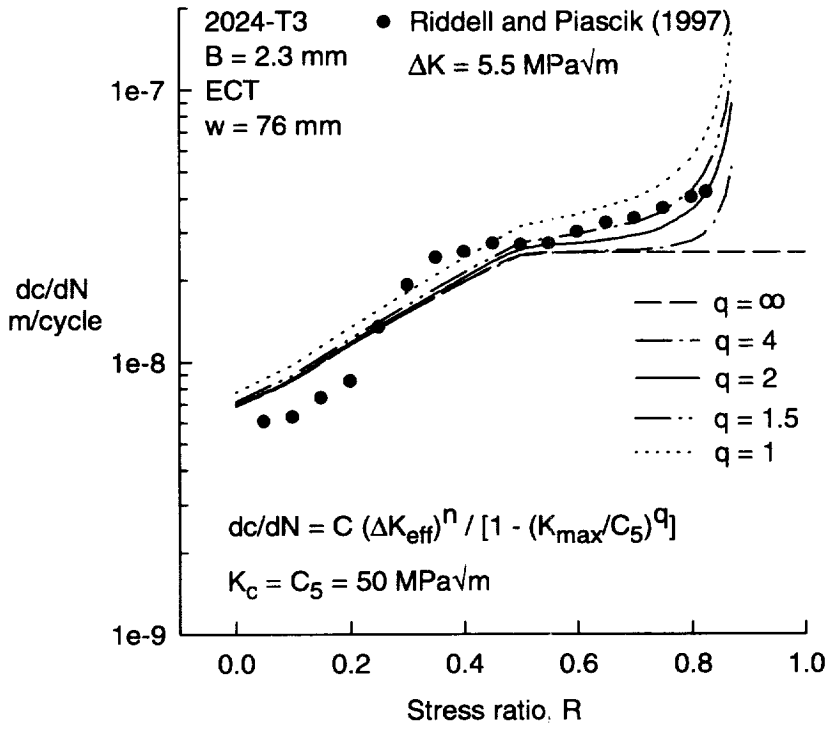


Figure 15. Influence of the power on $K_{max}/K_c$ ratio on crack-growth rates.

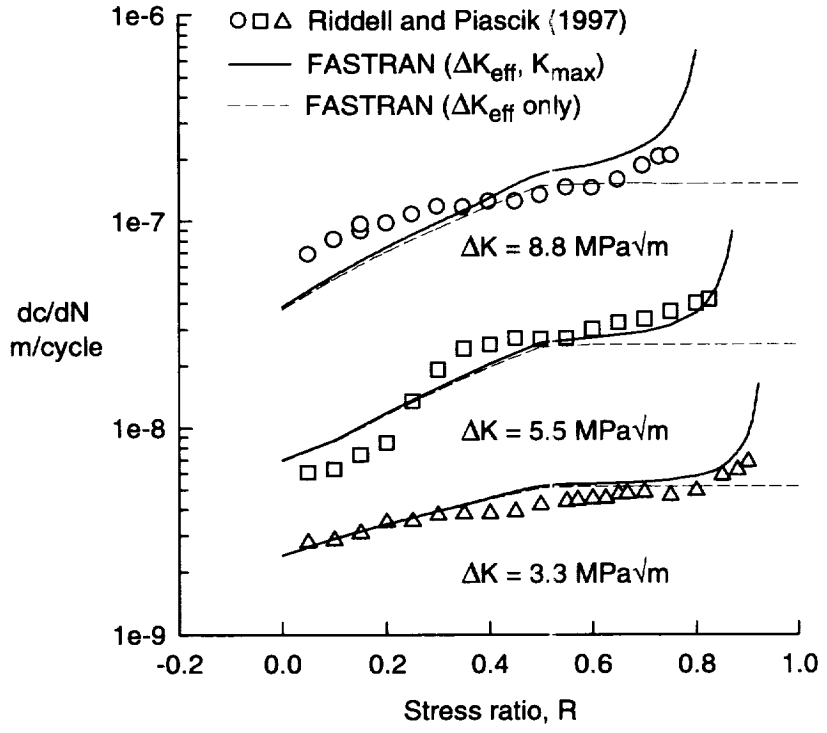


Figure 16. Comparison of measured and calculated rates for various ΔK values.

open symbols are high R ratio data (non-closure conditions from the analysis) and the solid symbols are low R ratio data. The dotted curve is the $\Delta K_{eff}$ baseline curve, an extension of the baseline curve from Figure 11, developed from data by Hudson [29] and Phillips [30]. Below a rate of 1E-7 m/cycle, plane-strain conditions prevail ($\alpha = 2$) and for rates greater than 2.5E-6 m/cycle, plane-stress conditions prevail ($\alpha = 1$). (See reference 33 for further information about constraint variations for this material.) The solid and dashed curves are the predicted $\Delta K$ against rate results from FASTRAN for the specimens tested at low and high R ratios. These results show that $K_{max}$ or stress-level effects are present even at low stress ratios, if the tests are conducted at high applied stress levels, because the test data and predicted curve are not parallel to the baseline curve (dotted curve). Note that these tests were cycled to failure and that the cyclic fracture toughness $K_F$ (chosen to fit the asymptotes) is considerably higher than the static value ($K_F = 267$ MPa$\sqrt{m}$) reported in reference 31.

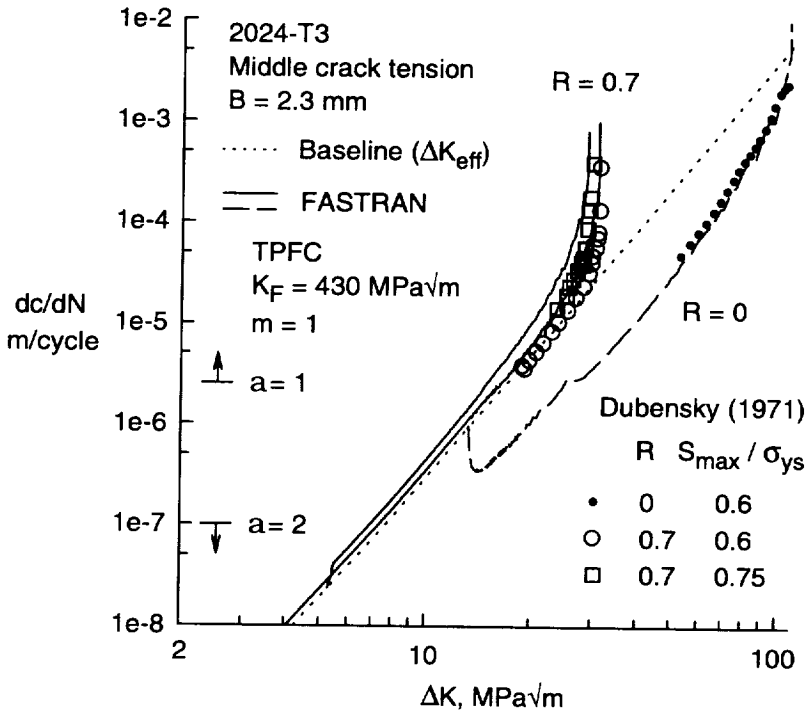


Figure 17. Measured and calculated crack-growth rates for high stress levels at low and high stress ratios on an aluminum alloy.

In efforts to determine the appropriate crack-driving parameters, Vasudevan and Sadananda [4,5] and Donald et al. [7,23] are plotting $\Delta K$ against $K_{max}$ at constant crack-growth rates, as shown in Figure 18. These data (symbols) were obtained from Donald [23] on 2024-T351 aluminum alloy compact specimens tested at a very high humidity. These tests were conducted under the $\Delta K$-reduction procedure (ASTM E-647-95a) which may induce other forms of closure, such as roughness or oxide-debris, in addition to plasticity from load-history effects. This crack-growth rate (5.2E-9 m/cycle) is slightly above the threshold region for this alloy. The effective stress-intensity factor range against rate baseline curve for this material and humidity were obtained from the R = 0.7 results ($\Delta K = \Delta K_{eff}$). The curves are calculated from the plasticity-induced crack-closure model for various values of constraint. Plane-strain conditions, such as $\alpha = 2$, are expected to prevail at the low crack-growth rate but lower values of $\alpha$ are required to fit the test data. These results illustrate a deficiency with the current plasticity model, in that, other forms of closure such as fretting-oxide-debris- and roughness-induced closure are not accounted for in the model. At present,

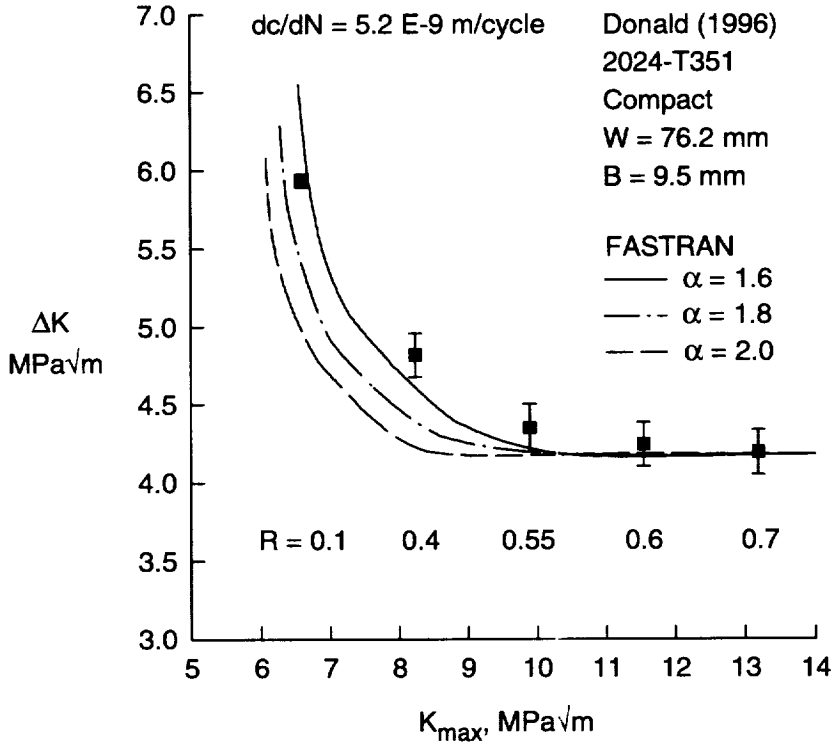


Figure 18. Measured and calculated crack-growth rates on an aluminum alloy under high humidity near threshold conditions.

a higher value of $\alpha$ is required to account for these additional sources of closure. Further study is needed in the threshold regime to develop a model which includes the three major forms of closure.

## CONCLUSIONS

(1) For small-scale yielding conditions, the $\Delta K_{eff}$ crack-growth rate relation is directly related to the effective cyclic crack-tip-opening displacement ($\Delta\delta_{eff}$) over a wide range of stress ratios (-1 to 0.8) for a aluminum alloy and steel.

(2) Based on the cyclic crack-tip hysteresis energy and the plasticity-induced crack-closure model, the crack-tip damage for applied stresses less than the "crack-opening" stress is negligible (less than 5 percent affect on crack-growth rates) for the Paris crack-growth regime.

(3) The compliance offset method (for 1 to 2% offset) measures significantly lower crack-opening stresses than physically occur in the crack-closure model.

(4) The effective stress-intensity factor range calculated from the crack-closure model for the adjusted compliance ratio method produces crack-growth rate trends opposite from those calculated from the traditional method for a crack initiating from a sawcut or notch.

(5) Effects of $K_{max}$ on crack-growth rates can become significant when the specimen size becomes small (elastic fracture toughness becomes small), as stress ratios approach unity, and as the $K_{max}/K_c$ ratio becomes greater than about 0.5.

## REFERENCES

[1] Elber, W., "The Significance of Fatigue Crack Closure," Damage Tolerance in Aircraft Structures, ASTM STP 486, American Society for Testing and Materials, 1971, pp. 230-242.

[2] Walker, N. and Beevers, C. J., "A Fatigue Crack Closure Mechanism in Titanium," Fatigue of Engineering Materials and Structures, Vol. 1, No. 1, 1979, pp. 135-148.

[3] Paris, P. C., Bucci, R. J., Wessel, E. T., Clark, W. G. and Mager, T. R., "Extensive Study of Low Fatigue Crack Growth Rates in A533 and A508 Steels, " ASTM STP-513, 1972, pp. 141-176.

[4] Vasudevan, A. K. and Sadananda, K., "Classification of Fatigue Crack Growth Behavior," Metallurgical and Materials Transactions A, Vol. 26A, May 1995, pp. 1221-1234.

[5] Sadananda, K. and Vasudevan, A. K., "Analysis of Fatigue Crack Closure and Thresholds," Fracture Mechanics: 25th Volume, ASTM STP 1220, F. Erdogan, Ed., American Society for Testing and Materials, 1995, pp. 484-501.

[6] Chen, D. L., Weiss, B. and Stickler, R., "A New Evaluation Procedure for Crack Closure," International Journal of Fatigue, Vol. 13, No. 4, 1991, pp. 327-331.

[7] Donald, J. K., Bray, G. H. and Bush, R. W., "An Evaluation of the Adjusted Compliance Ratio Technique for Determining the Effective Stress Intensity Factor," Fracture Mechanics: 29th Volume, ASTM STP 1331, T. L. Panontin and S. D. Sheppard, Eds., American Society for Testing and Materials, 1997.

[8] Marci, G., "Failure Mode below 390K with IMI 834," Fatigue '96 Proceedings of the Sixth International Fatigue Congress, Berlin , Germany, G. Lütjering and H. Nowack, Eds., Vol. I, pp. 493-498.

[9] Riddell, W. and Piascik, R. S., "Stress Ratio Effects on Crack Opening Loads and Crack Growth Rates in Aluminum Alloy 2024," Fracture Mechanics: 29th Volume, ASTM STP 1331, T. L. Panontin and S. D. Sheppard, Eds., American Society for Testing and Materials, 1997.

[10] Weertman, J., "Rate of Growth of Fatigue Cracks Calculated from the Theory of Infinitesimal Dislocations Distributed on a Crack Plane," International Journal of Fracture, Vol. 2, 1966, pp. 460-467.

[11] Tomkins, B., "Fatigue Crack Propagation - An Analysis," Philosophical Magazine, Vol. 18, 1968, pp. 1041-1066.

[12] Ogura, K., Miyoshi, Y. and Nishikawa, I., "Fatigue Crack Growth and Closure of Small Cracks at the Notch Root," Current Research on Fatigue Cracks, T. Tanaka, M. Jono and K. Komai, Eds., Society of Materials Science, Japan, 1985, pp. 57-78.

[13] Dowling, N. E. and Begley, J. A., "Fatigue Crack Growth during Gross Plasticity and the J-Integral," Mechanics of Crack Growth, ASTM STP 590, American Society for Testing and Materials, 1976, pp. 82-103.

[14] Dugdale, D. S., "Yielding of Steel Sheets containing Slits," Journal of the Mechanics and Physics of Solids, Vol. 8, 1960, pp. 100-104.

[15] Newman, J. C., Jr., "A Crack-Closure Model for Predicting Fatigue Crack Growth under Aircraft Spectrum Loading," Methods and Models for Predicting Fatigue Crack Growth under Random Loading, ASTM STP 748, J. B. Chang and C. M. Hudson, Eds., American Society for Testing and Materials, 1981, pp. 53-84.

[16] Newman, J. C., Jr., "FASTRAN-II - A Fatigue Crack Growth Structural Analysis Program, NASA TM 104159, February 1992.

[17] Blom, A. R.; Wang, G. S. and Chermahini, R. G., "Comparison of Crack Closure Results Obtained by 3D Elastic-Plastic FEM and Modified Dugdale Model," Localized Damage: Computer-Aided Assessment and Control, M. H. Aliabadi et al., Eds., Computational Mechanics Publications, Springer-Verlag, Berlin, 1990, pp. 57-68.

[18] Newman, J. C., Jr., "Finite-Element Analysis of Crack Growth under Monotonic and Cyclic Loading," Cyclic Stress-Strain and Plastic Deformation Aspects of Fatigue Crack Growth, ASTM STP 637, American Society for Testing and Materials, 1977, pp. 56-80.

[19] Bichler, C. and Pippan, R., "Direct Observation of the Residual Plastic Deformation Caused by a Single Tensile Overload," Advances in Fatigue Crack Closure Measurement and Analysis, ASTM STP 1343, R. C. McClung and J. C. Newman, Jr., Eds., American Society for Testing and Materials, 1998.

[20] Chermahini, R. G., Shivakumar, K. N. and Newman, J. C., Jr., "Three-Dimensional Finite-Element Simulation of Fatigue Crack Growth and Closure," Mechanics of Fatigue Crack Closure, ASTM STP 982, J. C. Newman, Jr. and W. Elber, Eds., American Society for Testing and Materials, 1988, pp. 398-413.

[21] Riddell, W. T., Piascik, R. S., Sutton, M. A., Zhao, W., McNeill, S. R. and Helm, J. D., "Determining Fatigue Crack Opening Loads from Near-Crack-Tip Displacement Measurements," Advances in Fatigue Crack Closure Measurement and Analysis, ASTM STP 1343, R. C. McClung and J. C. Newman, Jr., Eds., American Society for Testing and Materials, 1998.

[22] Elber, W., "Crack-Closure and Crack-Growth Measurements in Surface-Flawed Titanium Alloy Ti-6Al-4V," NASA TN D-8010, September 1975.

[23] Donald, J. K., "Introducing the Compliance Ratio Concept for Determining Effective Stress Intensity," First International Conference on Fatigue Damage in Structural Materials," Hyannis, MA, September 22-27, 1996.

[24] Broek, D., "The Propagation of Fatigue Cracks Emanating from Holes," National Aerospace Laboratory, NLR Technical Report 72134U, 1972.

[25] Wu, Yisheng and Schijve, J., "Fatigue Crack Closure Measurements on 2024-T3 Sheet Specimens," Fatigue and Fracture of Engineering Materials and Structures Journal, Vol. 18, 1995, pp. 917-921.

[26] Newman, J. C., Jr., "Crack Growth under Variable Amplitude and Spectrum Loading in 2024-T3 Aluminum Alloys," Proceedings of the Symposium on High Cycle Fatigue of Structural Materials, TMS-ASM Fall Meeting, Indianapolis, IN, September 16-18, 1997.

[27] Paris, P. C. and Erdogan, F., "Critical Analysis of Crack Propagation Laws," Transaction of ASME, Journal of Basic Engineering, Vol. 85, 1963, pp. 528-534.

[28] Dubensky, R. G., "Fatigue Crack Propagation in 2024-T3 and 7075-T6 Aluminum Alloys at High Stress," NASA CR-1732, 1971.

[29] Hudson, C. M., "Effect of Stress Ratio on Fatigue-Crack Growth in 7075-T6 and 2024-T3 Aluminum Alloy Specimens," NASA TN D-5390, 1969.

[30] Phillips, E. P., "The Influence of Crack Closure on Fatigue Crack Growth Thresholds in 2024-T3 Aluminum Alloy," Mechanics of Fatigue Crack Closure, ASTM STP 982, J. C. Newman, Jr. and W. Elber, Eds., American Society for Testing and Materials, 1988, pp. 505-515.

[31] Newman, J. C., Jr., "Fracture Analysis of Various Cracked Configurations in Sheet and Plate Materials," Properties Related to Fracture Toughness, ASTM STP 605, American Society for Testing and Materials, 1976, pp. 104-123.

[32] Piascik, R. S. and Newman, J. C., Jr., "An Extended Compact Tension Specimen for Fatigue Crack Growth and Fracture Testing," International Journal of Fracture, Vol. 76, 1996, pp. R43-R48.

[33] Newman, J. C., Jr., "Effects of Constraint on Crack Growth under Aircraft Spectrum Loading," Fatigue of Aircraft Materials, A. Beukers, T. deJong, J. Sinke, A. Vlot and L. B. Vogelesang, Eds., Delft University Press, 1992, pp. 83-109.

| REPORT DOCUMENTATION PAGE | | Form Approved OMB No. 0704-0188 |
|---|---|---|



| 1. AGENCY USE ONLY (Leave Blank) | 2. REPORT DATE | 3. REPORT TYPE AND DATES COVERED |
|---|---|---|
| | August 1998 | Technical Memorandum |

**4. TITLE AND SUBTITLE**
An Evaluation of the Plasticity-Induced Crack-Closure Concept and Measurement Methods

**5. FUNDING NUMBERS**
WU 538-02-10-01

**6. AUTHOR(S)**
James C. Newman, Jr.

**7. PERFORMING ORGANIZATION NAME(S) AND ADDRESS(ES)**
NASA Langley Research Center
Hampton, VA 23681-2199

**8. PERFORMING ORGANIZATION REPORT NUMBER**
L-17748

**9. SPONSORING/MONITORING AGENCY NAME(S) AND ADDRESS(ES)**
National Aeronautics and Space Administration
Washington, DC 20546-0001

**10. SPONSORING/MONITORING AGENCY REPORT NUMBER**
NASA/TM-1998-208430

**11. SUPPLEMENTARY NOTES**
Paper presented at the ASTM Second Symposium on Advances in Crack Closure Measurement and Analysis (ASTM STP 1343) in San Diego, CA, November 13-14, 1997.

**12a. DISTRIBUTION/AVAILABILITY STATEMENT**
Unclassified-Unlimited
Subject Category 24 Distribution: Standard
Availability: NASA CASI (301) 621-0390

**12b. DISTRIBUTION CODE**

**13. ABSTRACT** (Maximum 200 words)

An assessment of the plasticity-induced crack-closure concept is made, in light of some of the questions that have been raised on the validity of the concept, and the assumptions that have been made concerning crack-tip damage below the crack-opening stress. The impact of using other crack-tip parameters, such as the cyclic crack-tip displacement, to model crack-growth rate behavior was studied. Crack-growth simulations, using a crack-closure model, showed a close relation between traditional $\Delta K_{eff}$ and the cyclic crack-tip displacement ($\Delta\delta_{eff}$) for an aluminum alloy and a steel. Evaluations of the cyclic hysteresis energy demonstrated that the cyclic plastic damage below the crack-opening stress was negligible in the Paris crack-growth regime. Some of the standard and newly proposed remote measurement methods to determine the "effective" crack-tip driving parameter were evaluated on middle-crack tension specimens. A potential source of the $K_{max}$ effect on crack-growth rates was studied on an aluminum alloy. Results showed that the ratio of $K_{max}$ to $K_c$ had a strong effect on crack-growth rates at high stress ratios and at low stress ratios for very high stress levels. The crack-closure concept and the traditional crack-growth rate equations were able to correlate and predict crack-growth rates under these extreme conditions.

**14. SUBJECT TERMS**
Fatigue crack growth; Fracture mechanics; Cracks; Stress-intensity factor; Crack closure; Plasticity; Constraint

**15. NUMBER OF PAGES**
31

**16. PRICE CODE**
A03

| 17. SECURITY CLASSIFICATION OF REPORT | 18. SECURITY CLASSIFICATION OF THIS PAGE | 19. SECURITY CLASSIFICATION OF ABSTRACT | 20. LIMITATION OF ABSTRACT |
|---|---|---|---|
| Unclassified | Unclassified | Unclassified | |